The Astronomical Journal, 156:152 (11pp), 2018 October https://doi.org/10.3847/1538-3881/aadb91


# Evolutionary Characteristics of the Interplanetary Magnetic Field Intensity

N. B. Xiang[1,2,3] and Z. N. Qu[4]
[1] Yunnan Observatories, Chinese Academy of Sciences, Kunming 650011, People's Republic of China; nanbin@ynao.ac.cn
[2] Center for Astronomical Mega-Science, Chinese Academy of Sciences, 20A Datun Road, Chaoyang District, Beijing, 100012, People's Republic of China
[3] Key Laboratory of Solar Activity, National Astronomical Observatories, CAS, Beijing 100012, People's Republic of China
[4] Department of Physics, School of Science, Sichuan University of Science and Engineering, Zigong 643000, People's Republic of China
*Received 2017 June 29; revised 2018 August 16; accepted 2018 August 16; published 2018 September 12*

## Abstract

We use several mathematical methods, such as the continuous wavelet transform, the wavelet coherence (WTC), and the partial wavelet coherence, to investigate the distribution and oscillation periods of the daily interplanetary magnetic field (IMF) intensity as well as the connection between IMF fluctuations and solar activity indices (the magnetic plage strength index and the Mount Wilson sunspot index). The daily IMF intensity generally approximately follows a log-normal distribution that is directly related to the distribution of the active region flux. The short-term periods of the IMF are about 13.7, 27.6, 37.1, and 75.3 days. They are driven by the quasi-periodicity of the magnetic surges on the solar surface. The medium-term periods of 1.07 and 1.82 years need to be derived from the stochastic interaction of local fields and meridional flows, since coronal holes reflect the transport of the magnetic flux on the solar surface and variations in the meridional flow are seen in the heliosphere. The 10.9-year period is the Schwabe solar cycle and is to be mentioned first. The solar cycle variation of the IMF is not thought to be related to weak solar magnetic activity, but is dominated by the strong solar magnetic field activity seen on the disk, because the footpoints of the time-varying component of the interplanetary magnetic flux are rooted in regions that are located near the sources of coronal mass ejections that are related to active regions, while the constant component in the IMF is thought to initially and mainly come from the weak solar magnetic field activity. Finally, the slow variation of the IMF indicates that it may have a period of longer than 50 years.

*Key words:* Sun: activity – Sun: general – Sun: magnetic fields

## 1. Introduction

The solar magnetic is field stretched out and is transported by the solar wind in the heliosphere, and this forms the interplanetary magnetic field (IMF). Since it originates from the solar magnetic field and because the Sun rotates, the IMF twists into the shape of a Parker spiral (Parker 1958). This has been confirmed by observations made with satellites. The solar magnetic field is thought to be mostly directed along this spiral, either away from or toward the Sun. According to the polarity of the original solar magnetic field, the positive and negative polarities of the IMF intermittently form two or more sectors (the so-called sector structure) in the equatorial plane. The IMF was first measured by magnetometers on board satellites in 1962, and space-based measurements have continued for more than 50 years. The satellite measurements near Earth and the reconstructed time series show that the IMF varies on timescales of seconds to decades (even longer than several solar cycles), i.e., it varies from solar minimum to maximum, and from one cycle to the next. According to the observation records, the IMF intensity is much lower than the magnetic field strength on the solar surface: it is generally lower than 10 nT (see Figure 1). However, the variation in the IMF is very important to the Earth's magnetosphere. When the IMF encounters the Earth's magnetosphere, it continuously interacts with the geomagnetic field, which shows itself for example as compression, distortion, and magnetic reconnection. For instance, the magnetic reconnection between the IMF and the geomagnetic field can cause intense substorm/convection events (Dungey 1961; Gonzalez & Mozer 1974), which may affect telecommunications, power lines, navigation, etc.

Many papers have studied the reasons that cause the variation in the IMF direction and intensity, especially the instantaneous variation and dynamical evolution. The traditional understanding of the IMF direction as described by Parker (1958, 1963) is that a radial IMF is produced above the acceleration region by the rapid acceleration of the solar wind, which is then wound by solar rotation to produce the shape of a Parker spiral. This process may result in a radial IMF at 1 au, but not farther out. However, a nearly radial IMF in the interplanetary medium that lasted for 6 hr or longer was first described by Neugebauer et al. (1997), and these intervals of the radial IMF near 1 au are probably initially related with regions that trail behind interplanetary coronal mass ejections (ICMEs) and are later associated more strongly with periods in which the wind speed decreases. Because this interpretation is different from the traditional view, many studies, such as Jones et al. (1998), Wang et al. (2003), and Riley & Gosling (2007) studied this topic. Orlove et al. (2013) investigated the 226 intervals of nearly radial IMF orientations at 1 au that lasted longer than 6 hr, and the authors argued that the best interpretation of these intervals of a radial IMF is an interchange reconnection between two sources with different wind speeds.

Observations with the highest resolution made directly by satellites show that the IMF intensity varies at timescales of seconds. Souza et al. (2016) found that the main period of the $B_z$ component of the IMF is shorter than 8 hr, which is probably related to Alfvén waves. Generally, IMF intensity variations on timescales of a few days to years are mainly related to the latitudinal distribution and evolution of coronal holes and to photospheric magnetic fields (Neugebauer et al. 2000; Takalo & Mursula 2002; Mursula & Vilppola 2004; Vats 2012). Neugebauer et al. (2000) specifically reported that the synodic solar rotation period of 27.03 days detected in the radial IMF

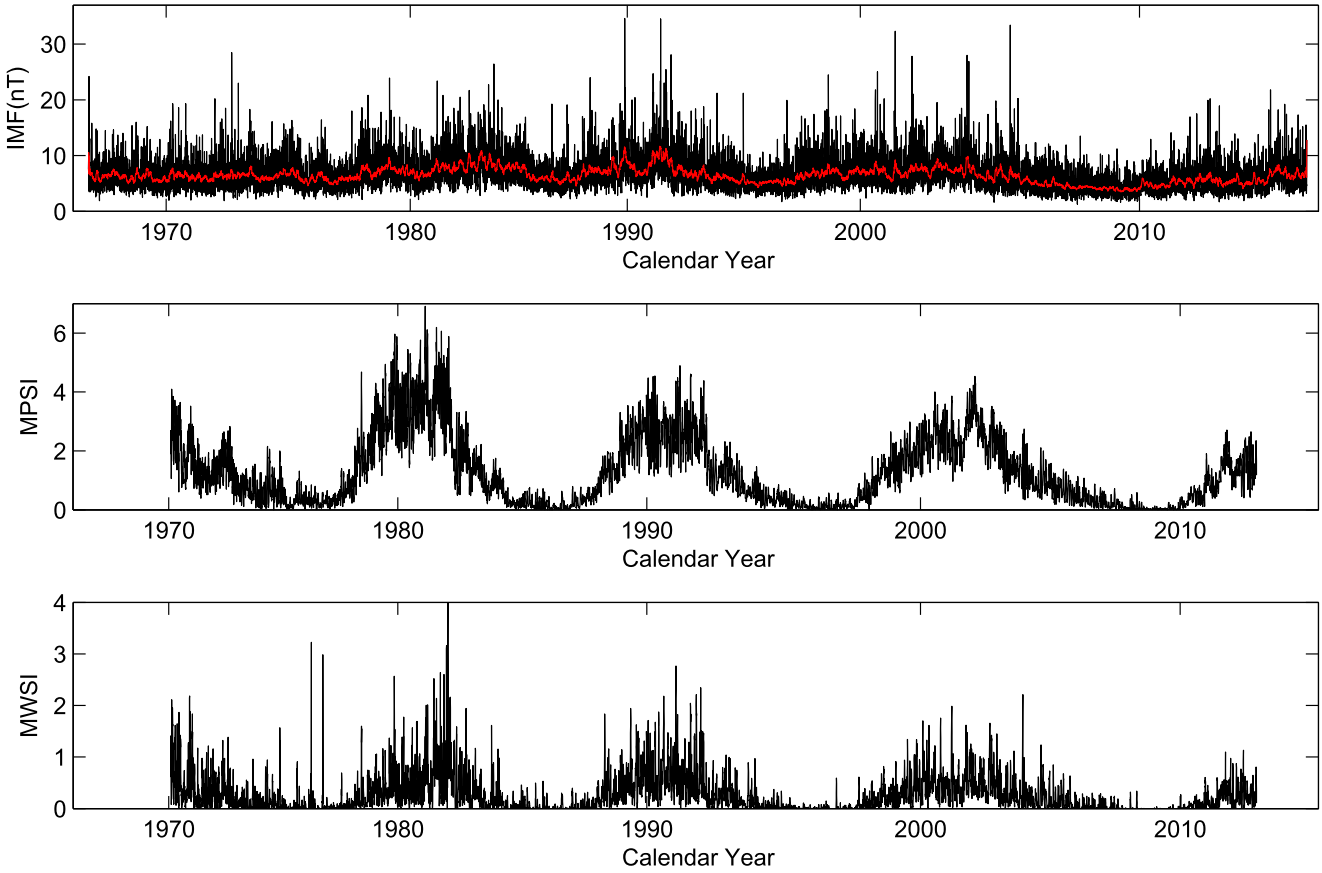


**Figure 1.** Top panel: Daily IMF intensity (black line) and smoothed 27-day averages (red line) from 1967 January 1 to 2015 December 31. Middle and bottom panel: Daily MPSI and MWSI from 1970 January 19 to 2013 January 31, respectively.

component is the most dominant rotation period over long time-intervals, and this signal is stronger for intervals of maxima and declining phases of solar activity than for intervals of low and ascending solar activity. Takalo & Mursula (2002) later described that the most persistent synodic solar rotation period found in the in-ecliptic IMF components is 27.6 days, which is somewhat longer than Neugebauer et al. (2000) suggested. Vats (2012) also indicated that the sidereal rotation period of the IMF varies from 24.1 to 25.8 days with an average value of about 25 days. Furthermore, the period of 153 days in the IMF at 1 au intermittently appeared with solar cycles, which may be related to a Reiger-type period (Cane et al. 1998). A period of about 1.7 years was detected in the IMF intensity at mid-latitudes, which was latitudinally organized (Mursula & Vilppola 2004). Moreover, a new period in the properties of the IMF intensity found by Takalo & Mursula (2002) was about 3.2 years, which is probably due to fluctuations in the heliospheric current sheet.

At timescales of a solar cycle, the IMF intensity shows a strong variation with the solar cycle that varies in phase with the sunspot numbers (Richardson et al. 2002a). However, the IMF intensity in the recent protracted solar minimum seems to be weaker than in past solar minima since 1963 (Smith & Balogh 2008; Connick et al. 2009, 2011). Schwadron et al. (2010) developed a theory of IMF flux generation and loss in which coronal mass ejections (CMEs) inject new magnetic flux into the heliosphere, which increases the IMF intensity, while the interchange reconnection of new magnetic flux with preexisting heliospheric magnetic flux occurs in interplanetary space, which leads to a decrease in the IMF intensity (Owens & Crooker 2006, 2007; Owens et al. 2008; Lockwood et al. 2009). The results from this model interpret the observed behavior well, including the IMF variation during the recent protracted solar minimum. Smith et al. (2013) used the sunspot number as a proxy for the CME eruption rate, and validated this model. The authors found that the predicted intensity is very consistent with the observed IMF.

This shows that early studies on the variation and dynamical evolution of the IMF investigated the radial IMF (or $B_z$ component) and the instantaneous variation in more detail. We also find that some interpretations of the periods and the reason for the variations in IMF intensity are not appropriate and new interpretations are needed, so that the evolutionary characteristics of the daily IMF intensity on timescales of several days to a Schwabe solar cycle still are an open issue. On the other hand, it is well known that the IMF is determined by the amount of solar magnetic flux that passes through the top of the solar corona into the heliosphere as well as the dynamical evolution of the magnetic flux in interplanetary space, which means that the IMF is rooted in the Sun's photosphere. The magnetic plage strength index (MPSI) and the Mount Wilson sunspot index (MWSI), which are based on full-disk solar magnetic magnetograms measured at the Mount Wilson Observatory (MWO) since the 1970s, are therefore introduced to reflect the full-disk solar magnetic activity (Howard et al. 1980, 1983; Chapman & Boyden 1986; Ulrich 1991; Ulrich et al. 1991; Parker et al. 1998). Consequently, we use MPSI and MWSI, and combine a variety of mathematical methods to study the distribution and evolutionary characteristics of more than 50 years of the daily IMF intensity observed

near Earth, and try to investigate the reasons that cause the variations in IMF intensity at different timescales.

## 2. Evolutionary Characteristics of the Daily IMF Intensity

### 2.1. Data

The IMF was systematically observed by various spacecraft on near-Earth orbits since 1963, and the daily IMF intensity was computed based on the basic hourly values. These records of the IMF intensity can be download from the OMNI (Operating Missions as a Node on the Internet) database of NASA (https://omniweb.gsfc.nasa.gov/form/dx1.html). Because there are too many days without measurements during 1963–1966, we select the daily IMF intensity from 1967 January 1 to 2015 December 31 in this study. Figure 1 (top panel) shows the daily IMF intensity (black line) in this time interval, and the smoothed 27-day averages are also shown in this panel (red line). The most striking feature of the daily IMF intensity is a sharp rise with a similar or even greater amplitude on short timescales. Another distinguishable feature of this time series is the variation with magnetic cycle. The smoothed 27-day averages, which can remove the short-term oscillations of this time series, indicate that it has multiscale oscillations on different timescales. Babcock (1953) built the first solar magnetograph and started full-disk observations at the MWO in the 1950s, but the early data are not available in digital format. The available full-disk magnetic magnetograms of the Sun in digital form were measured at the 150-foot high solar tower of the MWO since the 1970s (Chapman & Boyden 1986; Parker et al. 1998). Based on each magnetogram, an MPSI value and an MWSI value are calculated. To calculate the MPSI, all pixels in which the absolute value of the magnetic field strength is in the range of 10–100 G are first selected in the magnetogram. Then, the absolute values of the magnetic field strengths are summed for these selected pixels. Finally, this summation is divided by the total number of pixels (regardless of magnetic field strength) in the magnetogram. The MWSI values are determined with much the same method as the MPSI, but only pixels in which the absolute value of the magnetic field strength is greater than 100 G are taken into account for the summation (Howard et al. 1980, 1983; Ulrich 1991; Ulrich et al. 1991; Li et al. 2014; Xiang et al. 2014). The MPSI represents the weak solar magnetic field activity (with plage/facular regions and outside of sunspots), while the MWSI indicates the strong solar magnetic field activity seen on the disk (for more details, see Howard et al. 1980, 1983; Chapman & Boyden 1986; Ulrich 1991; Ulrich et al. 1991; Parker et al. 1998; Li et al. 2014; Xiang et al. 2014). The two indices are determined for every day since 1970 January 19. They terminate in 2013 January. MPSI and MWSI data from 1970 January 19 to 2013 January 31 are also displayed in the middle and bottom panel of Figure 1, respectively, and they can be downloaded from the MWO (http://obs.astro.ucla.edu/intro.html).

### 2.2. Distribution

The daily IMF intensity is covered by observation records for 15,948 days of the total 17,897 days from 1967 January 1 to 2015 December 31, and the number of days without observation accounts for 10.89%. The maximum and minimum values of the IMF intensity are 1.3 and 34.6 nT, respectively, while the mean value is 6.4 ± 2.8 nT. Early studies of the IMF intensity distribution found that the hourly average distribution of the magnetic field intensity in the heliosphere is approximately log-normal (Burlaga & King 1979; Slavin & Smith 1983; Burlaga & Ness 1998; Burlaga & Szabo 1999; Burlaga 2001, and references therein), although Feynman & Ruzmaikin (1994) did not agree with this conclusion. In this study, we use the longer IMF time series, which represent the daily averages of the IMF intensity at 1 au, to investigate the IMF intensity distribution. There are only 22 observation records shorter than 2 nT, which means about 0.14% of all days, and 32 observation values are higher than 21 nT, which is 0.21%. Thus, these lower or higher values are not taken into account for our study of the IMF intensity distribution. We divide the observation values from 2 to 21 nT into 38 IMF bands, each of which spans 0.5 nT, and then we calculate the probability density of the daily IMF intensity within each band, which is the probability of IMF observation values for each band divided by the span of the band. The result is displayed as the histogram in Figure 2. In order to derive a probability density function that can characterize the daily IMF intensity distribution more accurately, we first use a log-normal distribution to match the histograms in Figure 2. Following the early studies (Burlaga & Ness 1998; Burlaga 2001), a log-normal distribution of the IMF intensity can be written as

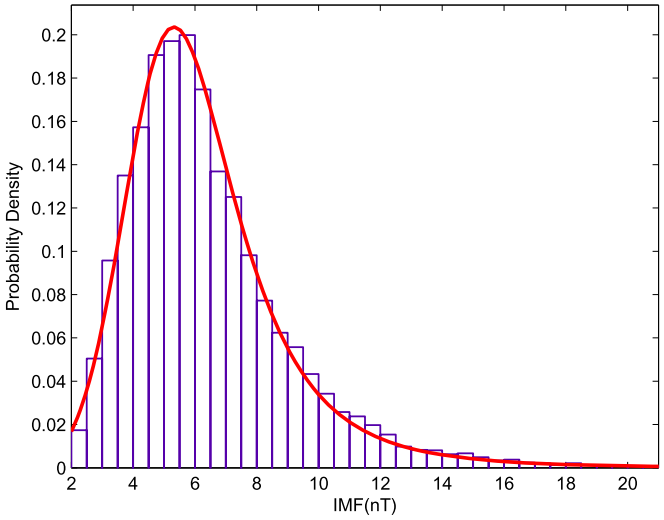


**Figure 2.** Histogram of the daily IMF intensity distribution. The distribution can be described quite well by the probability density function of the log-normal distribution (red line).

$$F = AB^{-1}e^{-\frac{(\ln B-\mu)^2}{2w^2}}, \quad (1)$$

where $\mu = \ln(BC)$ and $BC$ are parameters that are related to the most probable IMF intensity during the time interval considered, and $w$ describes the width of the distribution. Then, we also try to use other probability density functions, such as the $\Gamma$ distribution and the Student T distribution, to match the histogram in Figure 2. We find that this distribution is well characterized by the probability density function of the log-normal distribution. The result is also shown in Figure 2 (the smooth red line), and the function can be written as

$$f(x) = \frac{1}{0.8495x}e^{-\frac{(\ln x-1.8149)^2}{0.2297}}, \quad (2)$$

where $x$ represents the IMF intensity. On the other hand, it is known that the theoretical values of the skewness and kurtosis are zero if a distribution is truly normal. In practice, if the skewness and kurtosis of distribution of a time series are close to zero, this time series can still be characterized by a normal distribution, and this method has also been used in Feynman & Ruzmaikin (1994). Similarly, if the distribution of the daily IMF intensity is truly log-normal, the lower skewness and kurtosis (close to zero) of the distribution can be found, when the time series of logarithmic IMF intensity is used to calculate the skewness and kurtosis. For a time series $X_n$, $n = 1, \ldots, N$, the skewness and kurtosis of the distribution are defined as follows:

$$\text{skew} = \frac{1}{N}\sum_{i=1}^{N}\left(\frac{X_i - \overline{X}}{\sigma}\right)^3, \quad (3)$$

$$\text{kurt} = \frac{1}{N}\sum_{i=1}^{N}\left(\frac{X_i - \overline{X}}{\sigma}\right)^4 - 3, \quad (4)$$

where $\overline{X}$ and $\sigma$ indicate the average and standard deviation of the time series, respectively. Using the two definitions and the time series of the logarithmic IMF intensity, *skew* and *kurt* are 0.1563 and 0.0159, respectively. Hence, the two lower values also indicate that the distribution of the daily IMF intensity is approximately log-normal. Moreover, according to the probability density function (function 2), when $f(x)$ is maximum, x is about equal to 5.5 nT, which coincides with the observation records that show that the band 5–6 nT is the most productive for the IMF intensity during the time interval considered. This partly shows that this probability density function of the log-normal distribution is suitable for describing the distribution of this time series.

### 2.3. Periodicity of the IMF Intensity

The daily IMF intensity can be represented in the form of a time series $\{\text{IMF}_1, \text{IMF}_2, ..., \text{IMF}_n\}$, where the index of the first element is 1 and the last index is $n$. If the IMF is shifted by $d$ days with respect to itself, we can form $(n - d)$ pairs of observations from this series, $(\text{IMF}_1, \text{IMF}_{d+1})$, $(\text{IMF}_2, \text{IMF}_{d+2})$, ..., $(\text{IMF}_{n-d}, \text{IMF}_n)$. Then, we consider the first observation of each pair as one variable $\{\text{IMF}_1, \text{IMF}_2, ..., \text{IMF}_{n-d}\}$, and the second observation of each pair as the second variable $\{\text{IMF}_{d+1}, \text{IMF}_{d+2}, ..., \text{IMF}_n\}$. The autocorrelation coefficient $ACC(d)$ as a function is given by

$$\text{ACC}(d) = \frac{\sum_{i=1}^{n-d}(\text{IMF}_i - \overline{\text{IMF}})(\text{IMF}_{i+d} - \overline{\text{IMF}})}{\sum_{i=1}^{n+1-d}(\text{IMF}_i - \overline{\text{IMF}})^2}, \quad (5)$$

where $\text{IMF}_i$ indicates the $i$th element of the data sets $\{\text{IMF}_1, ..., \text{IMF}_n\}$, and the $d$ indicates the shift of the IMF with respect to itself. If there is no record of the IMF on a certain day, then the IMF value for that day is excluded from the calculation of the autocorrelation coefficient. Thus, the ACC is restricted to the available observation records and does not include any interpolations.

We calculate the autocorrelation coefficients of the relative phase shifts of the IMF with respect to itself for 1–5600 days. In order to clearly display the IMF periods, the ACC of the relative phase shifts of this time series with respect to itself for 6–5600 days and 6–450 days is shown in the left and right panels of Figure 3, respectively. We use a Monte Carlo method to test the statistical significance level of the ACC. The red dashed lines in the two panels indicate the 95% confidence level, and the correlation coefficients corresponding to these periods that are above the red dashed line in each panel are of statistical significance. As this figure shows, the short-term periods at a confidence level higher than 95% are 13, 28, 37, and 76 days. At timescales of a Schwabe solar cycle, it looks like there are several periods at a confidence level higher than 95% in the left panel of Figure 3, but the difference of these peak values is probably very small. Hence, we calculate the smoothed 365-day ACC averages, and the result is displayed as the blue solid line in the left panel of this figure. This helps us to obtain a more accurate Schwabe solar cycle of this time series: the Schwabe solar cycle with a confidence level higher than 95% is about 3974 days (10.88 years).

The wavelet analysis is widely used to detect time series periods and the localized oscillatory feature in time-frequency space (Torrence & Compo 1998; Grinsted et al. 2004; Li et al. 2005; Deng et al. 2013; Xie et al. 2017a, 2017b). When the wavelet is used for feature extraction purposes, the Morlet wavelet (dimensionless frequency $\omega_0 = 6$) is a good choice, since it is reasonably localized in both time and frequency (Torrence & Compo 1998; Grinsted et al. 2004). We used a continuous wavelet transform (CWT) to validate the IMF periods that are detected with the autocorrelation analysis. However, the wavelet is not completely localized in time, and the CWT suffers from edge artifacts. Thus, it is useful to introduce a cone of influence (COI) in which the wavelet power is caused by a discontinuity at the edges, which decreases by a factor $e^{-2}$ (Torrence & Compo 1998; Grinsted et al. 2004; Li et al. 2009; Xie et al. 2012).

The IMF intensity is systematically observed by various spacecraft near Earth orbit, but some days do not have observations. Especially, there are relative long and systematic gaps (generally shorter than six days) in the OMNI database during the 1980s, which may relate to the magnetospheric parts of the spacecraft orbit. In order to use the CWT, the cubic spline interpolation is used to interpolate the value when the IMF is absent on a certain day. The continuous wavelet power spectra of the daily IMF intensity and their corresponding 95% confidence level are given in the left panel of Figure 4. We can clearly see that the significant periods of the IMF are detected on a timescale of a few days to one Schwabe solar cycle. The short-term periods of statistical significance are intermittently detected around the sunspot maximum times, while the Schwabe solar cycle is of statistical significance in the entire time interval considered. We calculate the average of local "components" of continuous wavelet power spectra over time from 1967 January 1 to 2015 December 31, i.e., all time points of the left panel in Figure 4. The result indicates the global power spectra of this time series. In order to clearly show its peaks, which indicate the periods of daily IMF intensity, the global power spectrum is divided into three parts and the logarithmic global power is displayed. The global power spectra and their corresponding 95% confidence level are shown in the right panel of Figure 4. This shows that the peaks are centered around 13.7, 27.6, 37.1, 75.3, 390.1, 666.4, and 3993.8 days (10.93 years), all of which are above the 95% confidence level. We find that the medium-term periods of 390.1 and 666.4 days, which are about 1.07 and 1.82 years,

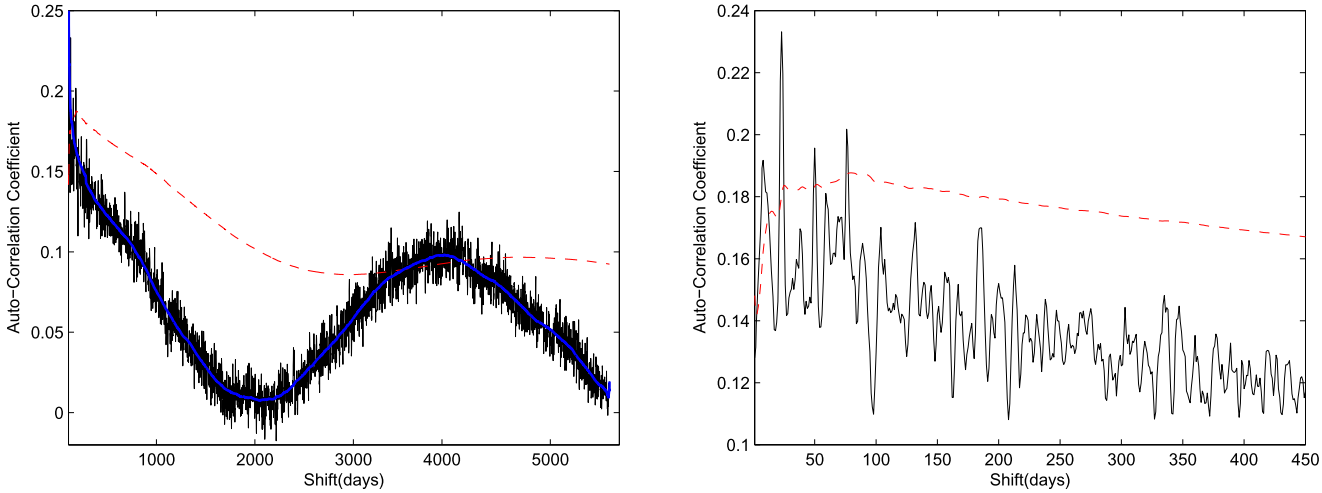


**Figure 3.** Left panel: Autocorrelation coefficients of relative phase shifts of the IMF with respect to itself for 6–5600 days. Right panel: Same as the left panel, but only for relative phase shifts for 6–450 days. The red dashed lines in two panels indicate the 95% confidence level. The correlation coefficients corresponding to these periods that are above the red dashed line in each panel are of statistical significance; the blue solid line in the left panel displays the smoothed 365-day ACC averages.

respectively, are only detected by the CWT because the autocorrelation analysis is not suitable for finding the medium-term periods of a time series. The oscillating signals of the time series are especially weak at medium-term timescales. Additionally, we cautiously check the gaps in the daily IMF intensity, and find that the time of the continuous data gaps is generally shorter than six days during the time interval considered, while the periods detected in this study are much longer than six days. In order to test the effect of these gaps on the results we found, we used another two methods to fill the data gaps: (i) the linear interpolation was used to interpolate the gaps, and (ii) the data gaps were filled by the average of their neighboring values of the IMF intensity. We find that when these two methods and the cubic spline interpolation are used to fill the gaps of the daily IMF intensity, almost the same periods are detected.

This shows that the short-term periods detected by the two methods show quite similar results, and the short-term periods of the IMF intensity are about 13.7, 27.6, 37.1, and 75.3 days. Many papers have indicated that the variations in the IMF might be strongly related to CMEs, solar wind, ICMEs, SSN, etc. (Richardson et al. 2002a, 2002b; Owens & Crooker 2006; Owens et al. 2008; Schwadron et al. 2010; Ahluwalia 2013; Smith et al. 2013). Furthermore, McIntosh et al. (2015) indicated that the magnetic surges from the activity bands show a quasi-periodicity that shapes the heliosphere and drives a host of energetic phenomena, such as flares, solar wind, and CMEs; and CMEs transport magnetic flux from the Sun toward the outer heliosphere in a quasi-periodic process that is similar to the periodic oscillation of the magnetic flux emergence and other eruptive solar activity (Low 1996; Lara et al. 2008). Consequently, we infer that these short-term periods of the IMF intensity are due to the quasi-periodicity of magnetic surges on the solar surface.

The medium-term periods are 390.1 and 666.4 days, which are about 1.07 and 1.82 years, respectively. The period of 1.07 years shows the annual variation of the IMF intensity. It is well known that the nearly annual period has a long history, but the origin is unclear so far. Many studies advised that the annual solar activity periods (indices) are caused by the annual change in the Earth's helio-latitude (Wilcox 1970; Wilcox & Scherrer 1972; Kotov 2006; Li et al. 2012; Xiang & Qu 2016). However, the continuous wavelet power spectra (left panel of Figure 4) displays that the annual IMF period is only detected in two intermittent time intervals of 1975–1980 and 1990–1995, which contain the time intervals of solar maximum and solar minimum. Consequently, we can infer that the annual variation of the IMF is not related to the annual change in the Earth's helio-latitude and is not related to the intensity of the solar magnetic field activity either. The other medium-term period of 1.82 years is also detected in these two intermittent time intervals. Wang & Sheeley (2003) gave a viable explanation for the quasi-periodicities of the magnetic field activity of the Sun in the range of 1–3 years that it is attributed to the stochastic interaction of local fields and meridional flows. Thus, the medium-term periods of 1.07 and 1.82 years detected in the IMF intensity might be related to the stochastic interaction of local fields and meridional flows.

When the autocorrelation analysis is used, the long period of the IMF intensity is 10.88 years. At the same time, a period of 10.93 years is detected using the CWT. The results from the two different methods are quite similar. This means that the long period of the IMF is about 10.9 years and corresponds to the solar cycle. In order to study the reason thats cause the variation in IMF intensity at timescales of a solar cycle, we investigate in the next section the relation of the IMF intensity with the MPSI and MWSI, which represent the weak and strong solar magnetic field activity, respectively, that is seen on the disk.

### *2.4. The Reason for the Inter-solar-cycle Variation of the IMF Intensity*

Wavelet coherence (WTC) is widely used to analyze the nonlinear behavior between two time series and to determine significant coherence even though the common power is low. The results from the WTC analysis can reveal the local correlation between two time series in time-frequency space (Grinsted et al. 2004; Deng et al. 2012; Xu et al. 2017). The WTC is briefly introduced as follows. For two time series $X_n$, $n = 1, \ldots, N$ and $Y_n$, $n = 1, \ldots, N$, the WTC can be defined as

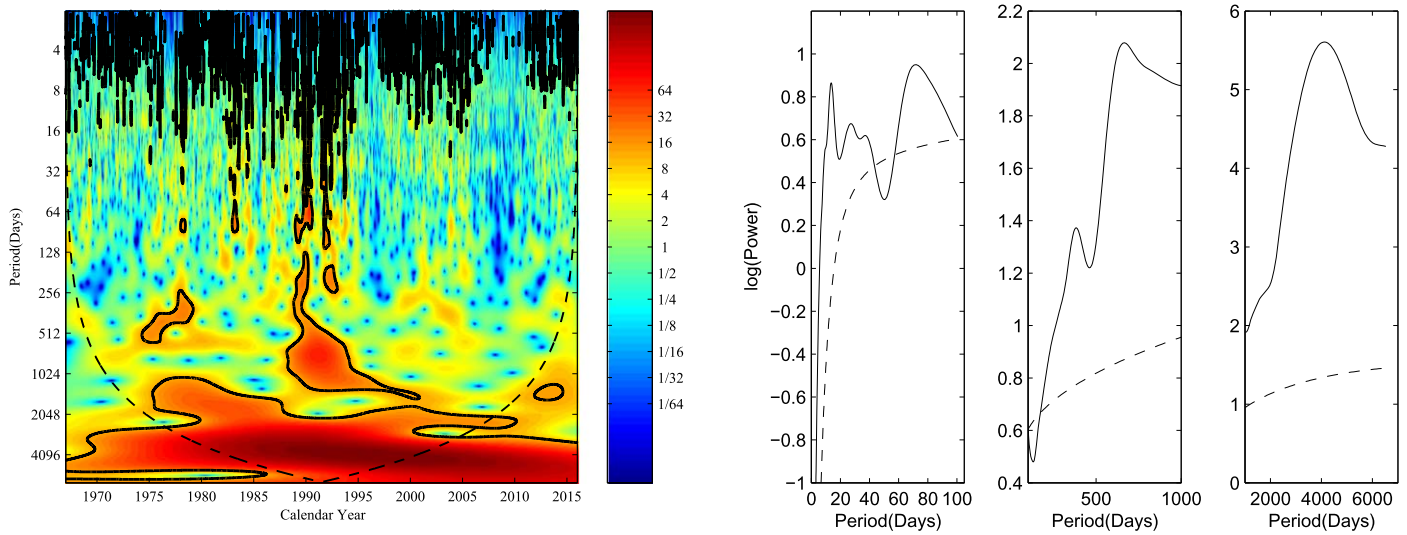


**Figure 4.** Left panel: Continuous wavelet power spectra of the daily IMF intensity from 1967 January 1 to 2015 December 31. The 95% confidence level is indicated by the thick black contours, and the dashed black line indicates the COI where edge effects might distort the picture. Right panel: Global power spectrum (solid lines) of the daily IMF intensity. The dashed lines show the 95% confidence level, and the periods indicated by the power spectrum peaks that are above the dashed lines are of statistical significance.

(Grinsted et al. 2004; Li et al. 2009)

$$R_n^2(s) = \frac{|S(s^{-1}W_n^{XY}(s))|^2}{S(s^{-1}|W_n^X(s)|^2) \cdot S(s^{-1}|W_n^Y(s)|^2)}, \quad (6)$$

where $W_n^X(s)$ indicates the wavelet transform of time series $X_n$, which can be represented as $W_n^X(s) = \sqrt{\frac{\delta t}{s}} \Sigma_{n'=1}^{N} X_{n'} \Psi_0[(n'-n)\frac{\delta t}{s}]$. In this function, $\delta t$ represents the uniform time step and $\Psi_0$ indicates the wavelet basis selected in the wavelet transform; accordingly, $s$ shows the variational scale of the wavelet when the wavelet is stretched in time. In this study, we select the Morlet wavelet, which can be defined as $\Psi_0(\eta) = \pi^{-1/4} e^{i\omega_0\eta} e^{-\frac{1}{2}\eta^2}$, where $\omega_0$ and $\eta$ are dimensionless frequency ($\omega_0 = 6$) and dimensionless time, respectively. Similarly, $W_n^Y(s)$ displayed in function (6) represents the wavelet transform of time series $Y_n$. $W_n^{XY}(s)$ shows the cross wavelet transform of the two time series $X_n$ and $Y_n$, and is defined as $W^{XY} = W^X W^{Y^*}$, where the asterisk denotes complex conjugation. Finally, $S$ shown in function (6) is a smoothing operator. The definition of the WTC closely resembles a traditional correlation coefficient. Hence, the results from the WTC analysis can be thought of as a local correlation between two time series in time-frequency space. In order to calculate the WTC spectra, the smoothing operator $S$ is displayed as the function

$$S(W) = S_{\text{scale}}(S_{\text{time}}(W_n(s))), \quad (7)$$

where $S_{\text{scale}}$ and $S_{\text{time}}$ denote smoothing along the wavelet scale axis and in time, respectively. Since the Morlet wavelet is selected in this study, a suitable smoothing operator can be defined as the following functions (Grinsted et al. 2004; Li et al. 2009):

$$S_{\text{time}}(W)|_s = (W_n(s) * c_1^{\frac{-t^2}{2s^2}})|_s \quad (8)$$

$$S_{\text{scale}}(W)|_n = (W_n(s) * c_2 \prod(0.6s))|_n, \quad (9)$$

where $c_1$ and $c_2$ are normalization constants, and $\prod$ is the rectangle function. For the Morlet wavelet, the factor 0.6 in function (9) is the empirically determined scale decorrelation length (Torrence & Compo 1998; Grinsted et al. 2004). In practice, both convolutions are made discretely, so that the normalization coefficients are determined numerically. Finally, the Monte Carlo method is used to estimate the statistical significance level of the WTC (Grinsted et al. 2004).

It is well known that partial correlation can estimate the degree of association between two random variables after eliminating the effect of a set of controlling random variables. Similarly, the partial wavelet coherence (PWC) can find the results of the WTC between two time series $y$ and $x_1$ after eliminating the effect of the time series $x_2$ (Ng & Chan 2012). The PWC squared of two time series $y$ and $x_1$ (after eliminating the effect of the time series $x_2$) can be defined as (Mihanović et al. 2009; Ng & Chan 2012)

$$RP^2(y, x_1, x_2) = \frac{|R(y, x_1) - R(y, x_2) \cdot R(y, x_1)^*|^2}{[1 - R(y, x_2)]^2 [1 - R(x_2, x_1)]^2}, \quad (10)$$

which is similar to the partial correlation squared and like the simple WTC, ranging from 0 to 1. In practice, because the WTC analysis of time series $y$ and $x_1$ displays a high squared at particular time-frequency space where a low $RP^2(y, x_1, x_2)$ was found, we can imply that the time series $x_1$ does not have a significant effect on the time series $y$ at that particular time-frequency space. In this study, the WTC (codes provided by Grinsted et al. 2004) is used to investigate the relation of the IMF with the MPSI and MWSI, respectively. Then we use the PWC (codes provided by Ng & Chan 2012) to find the results of the WTC analysis, and to try to investigate the reasons that cause the inter-solar-cycle variation of the IMF intensity.

The two indices (MPSI and MWSI), which have been measured since 1970, have no observation records accounting for about 27.8% from 1970 to 2013, so the two indices are an uneven time series. In order to use the CWT and PWC to analyze the relation of the IMF with the MPSI and MWSI, the

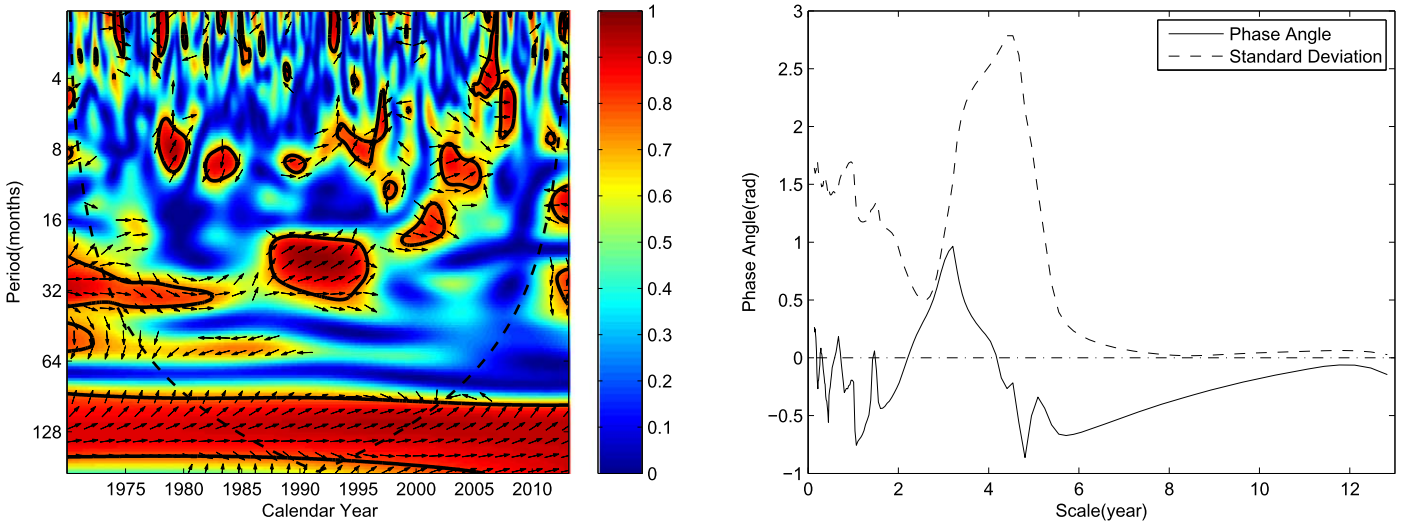


**Figure 5.** Left panel: Wavelet coherence of the monthly mean IMF and MPSI. The 95% confidence level is displayed as a thick contour, and the dashed black line indicates the COI where edge effects might distort the picture. The relative phase relation is shown as arrows (with in-phase pointing right, antiphase pointing left, and the IMF leading the MPSI by 90° pointing straight down). Right panel: Phase angles (solid line) of the IMF and MPSI as a function of the periods and their corresponding standard deviations (dashed line).

monthly mean values of three time series are needed. First, we select the days when the MPSI, MWSI, and IMF were all observed simultaneously from 1970 to 2013, and so three new time series that have the same observation days are obtained. Then, we calculate the monthly mean values of three new time series. There, the gaps in the three new time series are commonly random and shorter than 10 days, and the monthly means are used in order to have time series without data gaps. The WTC spectrum of the monthly mean IMF and MPSI, and the mean phase angle at a certain period scale are shown in the left and right panels of Figure 5, respectively. Here, the mean phase angle of two time series indicates the mean value of all phase angels at a certain period scale from the beginning to the end of the time interval considered. The WTC spectrum shows that the two series have a common significant region of above 95% confidence level at timescales of one solar cycle, but the mean phase angles of the IMF and MPSI at this timescale (about 10–12 years) are not negligible, although the value and the corresponding standard deviations are small. That is to say, the two time series should not be in phase at timescales of one solar cycle. Then, the PWC analysis is used to find the results of the WTC, and the results are shown in Figure 6. The PWC spectrum, which can find the results of the WTC between the IMF and MPSI (after eliminating the effect of the MWSI), indicates that the power is very low and the two time series have no common significant region at timescales of one solar cycle. Combining the WTC and PWC, we can infer that the solar cycle variation of the IMF intensity is not related to the solar weak magnetic field activity seen on the disk, which is represented by the MPSI.

We also use the WTC to analyze the relation of the IMF to the MWSI, and the results are shown in Figure 7. The WTC spectrum shown in the left panel of this figure indicates that the two time series have a common significant region of above 95% confidence level at timescales of one solar cycle. Furthermore, the mean phase angles of the IMF and MWSI and the corresponding standard deviation shown in the right panel of this figure are very small at this timescale (about 11 years). Hence, the IMF should be highly related and accurately in phase with the MWSI at timescales of one solar

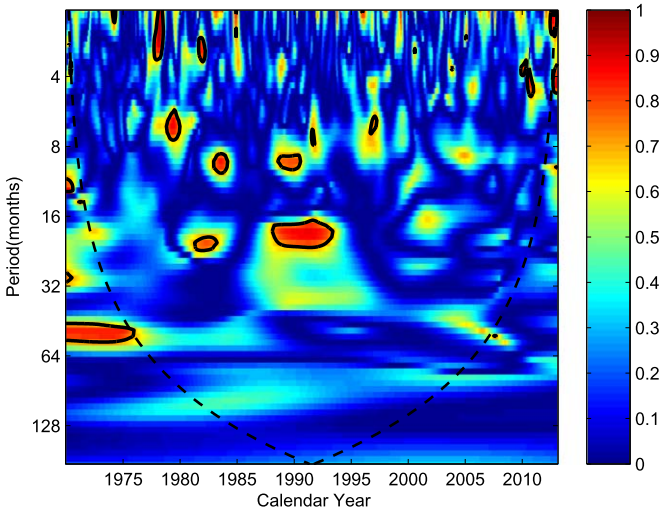


**Figure 6.** Partial wavelet coherence of the monthly mean IMF and MPSI. The 95% confidence level is shown as a thick contour, and the dashed black line indicates the COI where edge effects might distort the picture.

cycle. The PWC spectrum of the two time series is displayed in Figure 8, which can find the result of the WTC between the IMF and the MWSI after eliminating the effect of the MPSI. A common significant region of above 95% confidence level can be found in this figure at timescales of one solar cycle. Combining WTC and PWC, we infer that the variation of the IMF intensity at timescales of one solar cycle is probably highly related to the strong solar magnetic field activity seen on the disk, which is represented by the MWSI.

### *2.5. The Long-term Evolutionary Characteristics of the Daily IMF Intensity*

Many papers have investigated the slow variation of the IMF intensity that is thought to indicate the long-term evolutionary characteristics of this time series, but the different trend found in these studies may be due to the span of the time series as well as to the mathematical method (Lockwood et al. 1999; Stamper et al. 1999; Lockwood & Foster 2000;

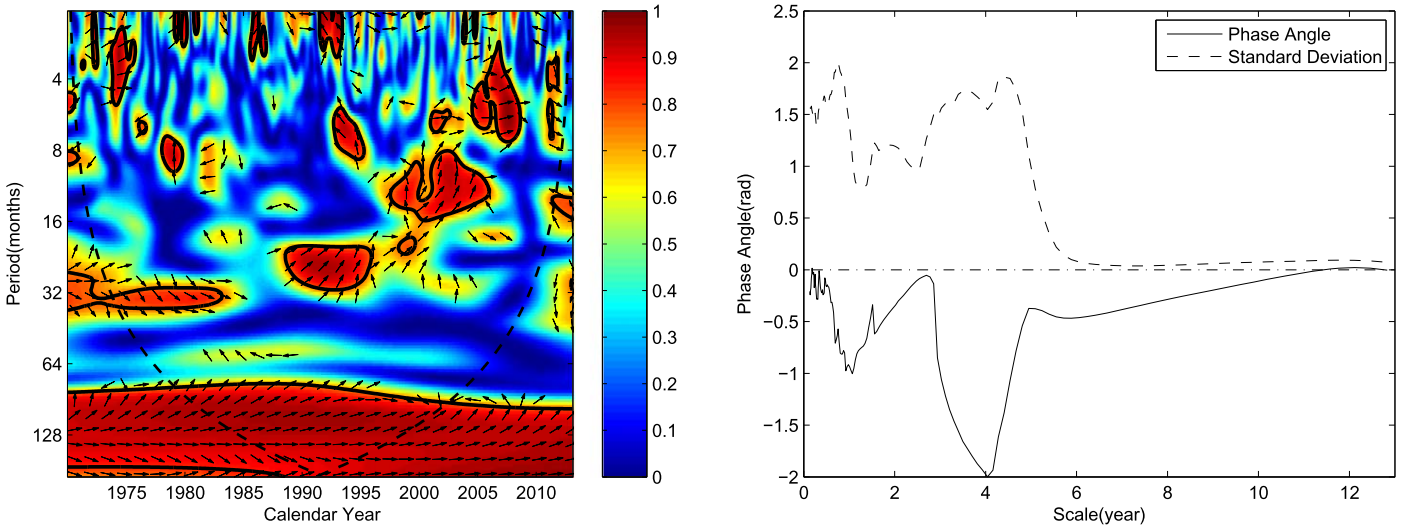


**Figure 7.** Left panel: Same as Figure 5, but for the WTC of the monthly mean IMF and MWSI. Right panel: Phase angles (solid line) of the IMF and MWSI as a function of the periods and their corresponding standard deviations (dashed line).

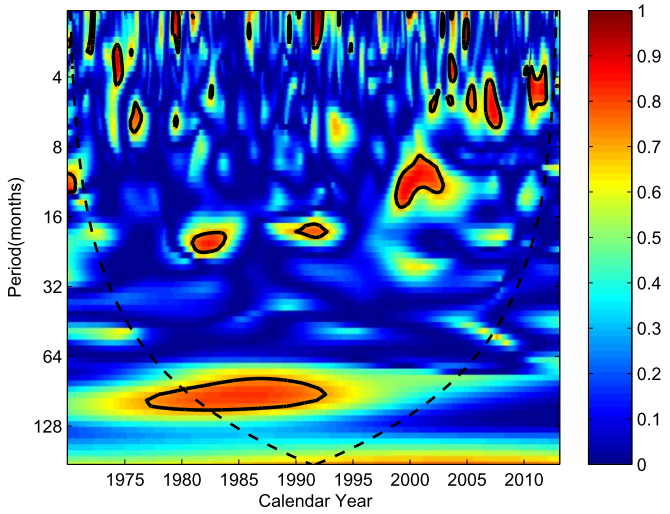


**Figure 8.** Same as Figure 6, but for the PWC of the monthly mean IMF and MWSI.

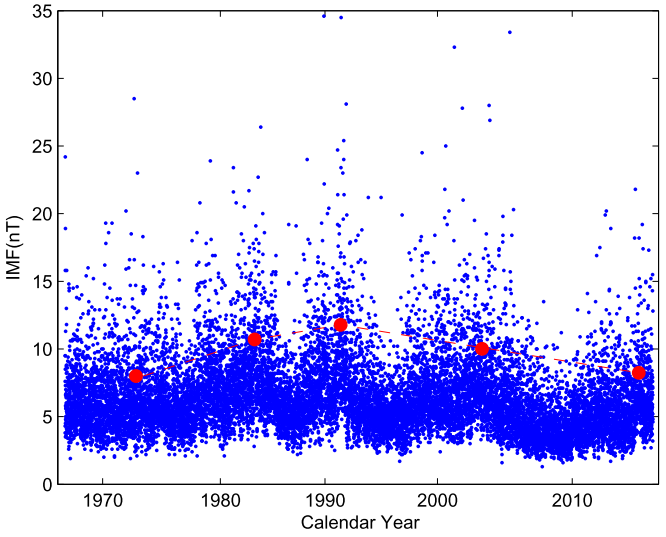


**Figure 9.** Long-term trend of the daily IMF intensity. Blue dots show the original records of the IMF intensity, red dots reflect the maximum IMF intensity in cycles 20–24, respectively, and the red dashed line connects these red dots.

Lockwood 2001; Richardson et al. 2002b). For instance, Lockwood et al. (1999) indicated that the radial component of the IMF near Earth increases by about 40% from 1964 to 1996. However, Richardson et al. (2002b) argued that the increase may be due to the lower than average fields during solar cycle 20 (1964–1976) in comparison with surrounding cycles, and the trend of the average IMF should show a slow decrease after 1976. Moreover, the IMF intensity through the prolonged solar minimum of cycle 24 shows weaker values than in the past solar minimum in the space age (Smith & Balogh 2008; Connick et al. 2009, 2011; McComas et al. 2013; Smith et al. 2013), and it continued to show these low values through the current solar mini-maximum (McComas et al. 2013; Smith et al. 2013). Here, the longer IMF time series through the prolonged solar minimum of cycle 24 and the current solar mini-maximum, which indicates a more long-term evolutionary characteristics of this time series, is used to investigate the long-term trend of the IMF intensity. We do not use the data-fitting method that is commonly used in the early papers, since the data-fitting mainly depends on the phase of the oscillation at the end and start of the data. Hence, we only compare the maximum time IMF intensity during the time interval of more than 50 years to derive the long-term trend of the daily IMF intensity. As a conventional definition of the solar maximum, based on the 12-month running means of the monthly mean values of the daily IMF intensity, we can obtain the maximum times of the IMF intensity in each cycle. Furthermore, the 12-month running means are expected to represent the general variation of the IMF intensity, and so the corresponding values of the 12-month running means at maximum times can reflect the maximum IMF intensity in each cycle, which is displayed as red dots in Figure 9. At the same time, the original records of the daily IMF intensity are also shown in this figure.

As Figure 9 shows, the red dots and dashed line obviously indicate the long-term trend of the daily IMF intensity. The trend of the daily IMF intensity shows a slow increase from cycles 20 to 22, and then slowly decreases from cycles 22 to 24. This variation trend indicates that the variation of the IMF

intensity may have a period longer than 50 years, although this period is statistically insignificant.

## 3. Conclusions and Discussion

The data used in this study are of the daily IMF intensity from 1967 January 1 to 2015 December 31, as listed in the OMNI database. A variety of mathematical methods, such as autocorrelation, CWT, WTC, and PWC, were used to study the evolutionary characteristics of more than 50 years of the daily IMF intensity as well as the reasons that cause the variation in IMF at different timescales.

The daily IMF intensity generally approximately follows the log-normal distribution during the time interval we considered. This distribution is consistent with early findings (Burlaga & King 1979; Burlaga & Ness 1998; Burlaga & Szabo 1999; Burlaga 2001, and references therein), although only the yearly distribution of the hourly averages of the magnetic field intensity in the heliosphere was discussed in these studies. However, Feynman & Ruzmaikin (1994) argued that the heliospheric magnetic field intensity does not exactly follow a log-normal distribution, since skewness and kurtosis of the logarithmic $B$ distribution are higher. Similarly, we find that the skewness and kurtosis are 0.1563 and 0.0159 in this study, respectively, which also indicates that the distribution of the daily IMF intensity during the time interval we considered is approximately log-normal. It is well known that the IMF is rooted in the Sun's photosphere, and Muñoz-Jaramillo et al. (2015) concluded that the flux distributions of photospheric magnetic structures is a linear combination of Weibull and log-normal distributions. Especially the pure Weibull and log-normal distributions can characterize the distribution of structures with fluxes below $10^{21}$ Mx and above $10^{22}$ Mx, respectively. That is to say, the Weibull distribution relates to decaying activity. It is strong evidence that shows that the daily IMF intensity distribution is directly related to the distribution of the active region flux. On the other hand, the skewness of 0.1563 reflects the right long tail that represents extreme events. Some authors also studied the part of the distribution of the heliospheric magnetic field intensities that is stronger than average and concluded that these stronger magnetic fields in the heliosphere can be approximately described by an exponential tail (Burlaga & Mish 1987; Burlaga & Ness 1996). Moreover, the nonzero skewness and kurtosis as well as the small departures of the histograms from the fitting curve as shown in Figure 2 indicate that deviations from a log-normal distribution are sometimes observed for the IMF intensity, especially for a strong IMF intensity. Burlaga (1991) suggested that the magnetic field intensity in the heliosphere observed by *Voyager 2* during 1987 and 1988 has a multifractal structure. We propse that the more exact distribution of the daily IMF intensity is probably a multifractal distribution, but we do not study the distribution in more detail here. Furthermore, another important study is how IMF distribution varies in time, which we also leave for future efforts. The multifractal distributions of the daily IMF intensity and the distribution variation in time will be the next study focus.

We used the autocorrelation analysis and CWT to detect the periods of the daily IMF intensity. As shown in Figures 3 and 4, the results from the two methods are quite similar. The short-term periods of the IMF are about 13.7, 27.6, 37.1, and 75.3 days. Neugebauer et al. (2000) reported that the most dominant rotation period detected in the radial component of IMF during long time-intervals is 27.03 days, which is due to the preferred-longitude effects. Takalo & Mursula (2002) in contrast argued that the most persistent synodic solar rotation period found in the in-ecliptic IMF components is 27.6 days, which is somewhat longer than Neugebauer et al. (2000) suggested. In this study, we used a longer time series of the daily IMF intensity (about 50 years), and find that the solar rotation period of the IMF is 27.6 days, which is consistent with the results in Takalo & Mursula (2002). We infer that the most accurate value of the most persistent solar rotation period of the IMF intensity probably is 27.6 days. Li et al. (2017) concluded that short-term periods of about 27, 13.5, and 9 days are clearly detected in the total as well as in low- and high-velocity solar wind, and the authors also interpreted the reasons for these short-term periods. For instance, they indicated that the reason for the rotation period of the solar wind is that the active regions and coronal holes from where solar wind is mainly emanated could usually last for more than one solar rotation. It seems that these short-term periods of the daily IMF intensity can be attributed to the periodic oscillation of the solar wind. However, many papers have indicated that the time-varying component in the interplanetary magnetic flux is related to the ejected associated flux carried by CMEs (McComas et al. 1992; Webb & Howard 1994; Owens & Crooker 2006, 2007; Owens et al. 2008; Schwadron et al. 2010; Smith et al. 2013). Moreover, McIntosh et al. (2015) indicated that a host of energetic phenomena, such as flares, solar wind, and CMEs, is driven by the magnetic surges from the activity bands, which show a quasi-periodicity at short timescales; and magnetic flux is carried by CMEs from the Sun toward the outer heliosphere in a quasi-periodic process that is similar to the periodic oscillation of the magnetic flux emergence and other solar eruptive activity (Low 1996; Lara et al. 2008). Consequently, we infer that a more plausible explanation is that these short-term periods of the daily IMF intensity are driven by the quasi-periodicity of magnetic surges on the solar surface.

Figure 4 also shows that the medium-term periods of the daily IMF intensity are 1.07 and 1.82 years. Wang & Sheeley (2003) gave a viable explanation for the quasi-periodicities of the magnetic field activity of the Sun in the range of 1–3 years: they attributed it to the stochastic interaction of local fields and meridional flows. It is well known that the meridional flows surge toward the poles or the equator in different phases of solar cycles. Observations have shown that the meridional flows have been found to vary over the solar cycle as well as from one solar cycle to the next, and can extend all the way to the poles (Basu & Antia 2010; Hathaway & Rightmire 2010, 2011; Rightmire-Upton et al. 2012). Moreover, early studies noted that the IMF variability is mainly related to the latitudinal distribution and evolution of coronal holes and related photospheric magnetic fields as well as to CMEs (Neugebauer et al. 2000; Takalo & Mursula 2002; Mursula & Vilppola 2004; Owens & Crooker 2006, 2007; Owens et al. 2008; Schwadron et al. 2010; Smith et al. 2013). Coronal holes reflect the transport of magnetic flux on the solar surface, and therefore variations in the meridional flows are seen in the heliosphere; CMEs are related to active regions, but the effect of CMEs is sporadic and their longitudinal distribution is more random. Hence, the two medium-term periods detected in the daily IMF intensity are due to the stochastic interaction of local fields and meridional flows.

Figures 3 and 4 show that the long period of the daily IMF intensity probably is about 10.9 years and corresponds to the solar cycle. Moreover, the results of the WTC and PWC of the IMF with the MPSI shown in Figures 5 and 6 display that the solar cycle variation of the daily IMF intensity is not related to the weak solar magnetic field activity, which is represented by the MPSI. Many researchers have suggested that the interplanetary magnetic flux consists of a constant open-flux component and a time-varying contribution that is related to the ejected associated flux carried by CMEs (McComas et al. 1992; Webb & Howard 1994; Owens & Crooker 2006, 2007; Owens et al. 2008; Schwadron et al. 2010; Smith et al. 2013). The constant open-flux component mainly originates from coronal holes, although some fraction of the magnetic flux seems to be related to an unknown source of quiet-Sun slow wind (Linker et al. 2017), since the coronal holes are generally regarded as the source of quiet-Sun fast solar wind (Waldmeier 1981; Das et al. 1993; Storini et al. 2006; Wang 2012; Li et al. 2016). In the interiors of coronal holes, slowly diverging flux tubes of open magnetic fields that are associated with fast solar wind are rooted, and these footpoint fields are rather weak and uniform. In the solar surface layer, Porter et al. (1987) and Martin (1988) found that the energy source for heating the corona and accelerating solar wind is probably derived from a dynamic network field with relatively weak strength. Li et al. (2016) also inferred that the disintegrated component of the strong solar magnetic field activity on the solar surface, which is the MPSI components coming from relatively early MWSI measurements (Xiang et al. 2014), heat coronal holes to emanate solar wind. Based on this analysis, we can infer that the constant open-flux component in the interplanetary magnetic flux that originates from coronal holes is initially derived from weak solar magnetic filed activity. Consequently, the constant component in the IMF intensity probably initially and mainly comes from the weak solar magnetic field activity seen on the disk, but the variation of the IMF intensity on timescales of one solar cycle is not attributed to this weak magnetic field activity, which is proved by the results of the WTC and PWC of the IMF with the MPSI (Figures 5 and 6).

The results of the WTC and PWC of the IMF with the MWSI shown in Figures 7 and 8 indicate that the variations of the IMF intensity on timescales of one solar cycle are probably highly related to the strong solar magnetic field activity seen on the disk, which is represented by the MWSI. The time-varying contribution, which is one of the two components in the interplanetary magnetic flux, is related to the ejected associated flux carried by CMEs (McComas et al. 1992; Webb & Howard 1994; Owens & Crooker 2006, 2007; Owens et al. 2008; Schwadron et al. 2010; Smith et al. 2013). At the same time, we also considered that CME magnetic clouds can lead to the short-term variability of interplanetary magnetic flux, but the more persistent increase in magnetic flux density in the heliosphere is due to "CME legs," which remain connected to the corona. The closed magnetic fluxes are dragged out by CMEs, which means that the footpoints of the time-varying component of the interplanetary magnetic flux are rooted in regions near the sources of CMEs, which are potentially located near active regions (strong magnetic field activity). The ejected associated contribution increases the IMF intensity, while the interchange reconnection and disconnection on different timescales decrease it (Owens & Crooker 2006; Owens et al. 2008; Schwadron et al. 2010). Moreover, the ejected associated contribution in the IMF is expected to display the solar cycle variation because of the CMEs that are related to active regions and sunspots. The balance between these processes allows the IMF intensity to display the solar cycle variation. Our study thus indicates that the variation of the daily IMF intensity on timescales of one solar cycle is dominated by the strong solar magnetic field activity seen on the disk.

Finally, we also investigated the long-term trend of the daily IMF intensity by comparing the maximum time of the IMF intensity during the time interval of more than 50 years. The trend of the IMF intensity shows a slow increase from cycles 20 to 22, and then displays a slow decrease from cycles 22 to 24. These long-term evolutionary characteristics indicate that the variation of the IMF intensity may have a period longer than 50 years, although this period is statistically insignificant, and more observation records are needed.

We thank the anonymous referee for their careful reading of the manuscript and for constructive comments that improved the original version. We also acknowledge the facilities OMNIWeb service and OMNI database of NASA as well as the staffs of this website. This study includes data (MPSI and MWSI) from the synoptic program at the 150-foot solar tower of the Mount Wilson Observatory. The Mount Wilson 150-foot solar tower is operated by UCLA, with funding from NASA, ONR, and NSF, under agreement with the Mount Wilson Institute. The authors are especially indebted to Dr. Ke-Jun Li for his constructive ideas and helpful suggestions on the manuscript. This work is supported by the National Natural Science Foundation of China (11573065, 11503082, 11633008, and 11603069), the Foundation of the Sichuan University of Science and Engineering grant 2015RC43, and the Chinese Academy of Sciences.

## References

Ahluwalia, H. S. 2013, AdSpR, 52, 2112
Babcock, H. W. 1953, ApJ, 118, 387
Basu, S., & Antia, H. M. 2010, ApJ, 717, 488
Burlaga, L. F. 1991, GeoRL, 18, 69
Burlaga, L. F. 2001, JGR, 106, 15917
Burlaga, L. F., & King, J. H. 1979, JGR, 84, 6633
Burlaga, L. F., & Mish, W. H. 1987, JGR, 92, 1261
Burlaga, L. F., & Ness, N. F. 1996, JGR, 101, 13473
Burlaga, L. F., & Ness, N. F. 1998, JGR, 103, 29719
Burlaga, L. F., & Szabo, A. 1999, SSRv, 87, 137
Cane, H. V., Richardson, I. G., & von Rosenvinge, T. T. 1998, GeoRL, 25, 4437
Chapman, G. A., & Boyden, J. E. 1986, ApJL, 302, L71
Connick, D. E., Smith, C. W., & Schwadron, N. A. 2009, ApJ, 695, 357
Connick, D. E., Smith, C. W., & Schwadron, N. A. 2011, ApJ, 727, 8
Das, T. K., Chatterjee, T. N., & Sen, A. K. 1993, SoPh, 148, 61
Deng, L., Qi, Z., Dun, G., & Xu, C. 2013, PASJ, 65, 11
Deng, L. H., Qu, Z. Q., Wang, K. R., & Li, X. B. 2012, AdSpR, 50, 1425
Dungey, J. W. 1961, PhRvL, 6, 47
Feynman, J., & Ruzmaikin, A. 1994, JGR, 99, 17645
Gonzalez, W. D., & Mozer, F. S. 1974, JGR, 79, 4186
Grinsted, A., Moore, J. C., & Jevrejeva, S. 2004, NPGeo, 11, 561
Hathaway, D. H., & Rightmire, L. 2010, Sci, 327, 1350
Hathaway, D. H., & Rightmire, L. 2011, ApJ, 729, 80
Howard, R., Adkins, J. M., Boyden, J. E., et al. 1983, SoPh, 83, 321
Howard, R., Boyden, J. E., & LaBonte, B. J. 1980, SoPh, 66, 167
Jones, G. H., Balogh, A., & Forsyth, R. J. 1998, GeoRL, 25, 3109
Kotov, V. A. 2006, SoPh, 239, 461
Lara, A., Borgazzi, A., Mendes, O., Jr., Rosa, R. R., & Domingues, M. O. 2008, SoPh, 248, 155

Li, K. J., Feng, W., Xu, J. C., et al. 2012, ApJ, 747, 135
Li, K. J., Gao, P. X., & Su, T. W. 2005, SoPh, 229, 181
Li, K. J., Gao, P. X., & Zhan, L. S. 2009, ApJ, 691, 537
Li, K. J., Kong, D. F., Liang, H. F., & Feng, W. 2014, AN, 335, 371
Li, K. J., Zhang, J., & Feng, W. 2017, MNRAS, 472, 289
Li, K. J., Zhanng, J., & Feng, W. 2016, AJ, 151, 128
Linker, J. A., Caplan, R. M., Downs, C., et al. 2017, ApJ, 848, 70
Lockwood, M. 2001, JGR, 106, 16021
Lockwood, M., & Foster, S. 2000, in The Solar Cycle and Terrestrial Climate, Solar and Space Weather, ESA SP 463, ed. A. Wilson (Noordwijk: ESA), 85
Lockwood, M., Rouillard, A. P., & Finch, I. D. 2009, ApJ, 700, 937
Lockwood, M., Stamper, R., & Wild, M. N. 1999, Natur, 399, 437
Low, B. C. 1996, SoPh, 167, 217
Martin, S. F. 1988, SoPh, 117, 243
McComas, D. J., Angold, N., Elliott, H. A., et al. 2013, ApJ, 779, 2
McComas, D. J., Gosling, J. T., & Phillips, J. L. 1992, JGR, 97, 171
McIntosh, S. W., Leamon, R. J., Krista, L. D., et al. 2015, NatCo, 6, 6491
Mihanović, H., Orlić, M., & Pasrić, Z. 2009, JMS, 78, S157
Muñoz-Jaramillo, A., Senkpeil, R. R., Windmueller, J. C., et al. 2015, ApJ, 800, 48
Mursula, K., & Vilppola, J. H. 2004, SoPh, 221, 337
Neugebauer, M., Goldstein, R., & Goldstein, B. E. 1997, JGR, 102, 19743
Neugebauer, M., Smith, E. J., Ruzmaikin, A., Feynman, J., & Vaughan, A. H. 2000, JGR, 105, 2315
Ng, Eric K. W., & Chan, Johnny C. L. 2012, JAtOT, 29, 1845
Orlove, S. T., Smith, C. W., Vasquez, B. J., et al. 2013, ApJ, 774, 15
Owens, M. J., & Crooker, N. U. 2006, JGRA, 111, A10104
Owens, M. J., & Crooker, N. U. 2007, JGRA, 112, A06106
Owens, M. J., Crooker, N. U., Schwadron, N. A., et al. 2008, GeoRL, 35, L20108
Parker, D. G., Ulrich, R. K., & Pap, J. M. 1998, SoPh, 177, 229
Parker, E. N. 1958, ApJ, 128, 664
Parker, E. N. 1963, Interplanetary dynamical processes (New York: Interscience Publishers)
Porter, J. G., Moore, R. L., Reichmann, E. J., Engvold, O., & Harvey, K. L. 1987, ApJ, 323, 380
Richardson, I. G., Cane, H. V., & Cliver, E. W. 2002a, JGRA, 107, 1187
Richardson, I. G., Cliver, E. W., & Cane, H. V. 2002b, JGRA, 107, 1304
Rightmire-Upton, L., Hathaway, D. H., & Kosak, K. 2012, ApJL, 761, L14
Riley, P., & Gosling, J. T. 2007, JGRA, 112, A06115
Schwadron, N. A., Connick, D. E., & Smith, C. 2010, ApJL, 722, L132
Slavin, J. A., & Smith, E. J. 1983, In Its Solar Wind Five, NASCP 2280 (Washington, D.C.: NASA), 323
Smith, C. W., Schwadron, N. A., & DeForest, C. E. 2013, ApJ, 775, 59
Smith, E. J., & Balogh, A. 2008, GeoRL, 35, L22103
Souza, A. M., Echer, E., Bolzan, M. J. A., & Hajra, R. 2016, JASTP, 149, 81
Stamper, R., Lockwood, M., Wild, M. N., & Clark, T. D. G. 1999, JGR, 104, 28325
Storini, M., Hofer, M. Y., & Sýkora, J. 2006, AdSpR, 38, 912
Takalo, J., & Mursula, K. 2002, GeoRL, 29, 1317
Torrence, C., & Compo, G. P. 1998, BAMS, 79, 61
Ulrich, R. K. 1991, AdSpR, 11, 217
Ulrich, R. K., Webster, L., Boyden, J. E., & Mangone, N. 1991, SoPh, 135, 211
Vats, H. O. 2012, P&SS, 63, 158
Waldmeier, M. 1981, SoPh, 70, 251
Wang, C., Richardson, J. D., Burlaga, L. F., & Ness, N. F. 2003, JGRA, 108, 1205
Wang, Y.-M. 2012, SSRv, 172, 123
Wang, Y.-M., & Sheeley, N. R., Jr. 2003, ApJ, 590, 1111
Webb, D. F., & Howard, R. A. 1994, JGR, 99, 4201
Wilcox, J. M. 1970, JGR, 75, 2587
Wilcox, J. M., & Scherrer, P. H. 1972, JGR, 77, 5385
Xiang, N. B., & Qu, Z. N. 2016, AJ, 151, 76
Xiang, N. B., Qu, Z. N., & Zhai, Q. 2014, AJ, 148, 12
Xie, J.-L., Shi, X.-J., & Xu, J.-C. 2012, RAA, 12, 187
Xie, J. L., Shi, X. J., & Xu, J. C. 2017a, AJ, 153, 171
Xie, J. L., Shi, X. J., & Zhang, J. 2017b, ApJ, 841, 42
Xu, J. C., Xie, J. L., & Qu, Z. N. 2017, ApJ, 851, 141